PCCP

Accepted Manuscript

ROYAL SOCIETY OF CHEMISTRY

www.rsc.org/pccp

Cite this: DOI: 10.1039/c0xx00000x

www.rsc.org/xxxxxx

ARTICLE TYPE

Steric matching and concentration induced self-assembled structural variety of 2,7-bis(*n*-alkoxy)-9-fluorenone at the aliphatic solvent/ graphite interface

Xinrui Miao,* Li Xu, Lihua Cui and Wenli Deng*

Received (in XXX, XXX) Xth XXXXXXXXX 20XX, Accepted Xth XXXXXXXXX 20XX
DOI: 10.1039/b000000x

Controlling and unraveling the structural polymorphism has been received special attention in 2D self-assembled monolayers. In this work, we investigated the steric matching and solution concentration controlled structural variety in self-assembly of 2,7-bis(n-alkoxy)-9-fluorenone (F−OC_n) at the *n*-tetradecane and *n*-tridecane/graphite interface under different concentrations, respectively. Scanning tunneling microscopy (STM) revealed that the coadsorbed adlayers of F−OC_n and solvents (n = 12−16) were formed and exhibited concentration dependent 2D phases due to the steric matching. The self-assembled monolayer of F−OC_n (n = 12−16) evolved from a low-density coadsorbed linear lamellar packing which was formed at low concentrations to higher-density patterns at relatively high concentrations. F−OC_{14} exhibited complex structural variety, in which a systematic trend of decrease in the molecular density per unit cell with decreasing concentration was obtained. Except for F−OC_n (n = 13, 15, 17), the zigzag structure showing the linear lamella with dimers was observed. The systematic experiments revealed that the self-assembly of F−OC_n had chain-length dependence. The results provide insight into the structural variety exhibited by a series of organic molecules and furnish important guidelines to control the morphology by changing the solution concentration.

1. Introduction

Supramolecular self-assembly has been established as an important concept for building functional monolayer patterns. The field of two-dimensional (2D) crystal engineering relates the adlayer arrangement with the nature of the substrate[1-2] and solvent,[3-4] concentration,[3, 5-6] temperature,[7-10] and the geometry and functionality of the adsorbed molecules.[11-17] So it is a great challenge to predict the thermodynamic equilibrium structure for a particular system. In addition, a simple system consisting of a combination of a single molecule and a solvent might display more than one self-assembled 2D pattern with varying level of the solvent coadsorption.[18-21] In most cases, the ratio of multiple structural phases is associated with changes in system parameters, such as solution concentration.[22] The phases could display transitions, which can be tracked by scanning tunneling microscopy (STM). To date, hydrogen bonding between molecule and solvent has been exploited to describe such system.[18, 23-24] For example, Zhang et al.[25] reported that 1-octanol could induce a series of symmetric and structural transitions on the monodendron 5-(benzyloxy)-isophthalic acid derivative molecular self-assembly. Despite the number of studies about solvent-induced self-assembly at the liquid-solid interface is relatively few. However, developing a compound showing the ability to exist in multiple 2D phases due to different molecule−solvent interactions is essential to study polymorphic phenomenon.

Molecular shape, size, structure, and nature of molecular substituent are key factors governing the formation of self-assembled nanostructures. So the complex intermolecular interactions could benefit for the formation of polymorphic structures. In our previous work, we found that the self-assembly of 2,7-bis(*n*-alkoxy)-9-fluorenone (F−OC_n, *n* = 12−18, Scheme 1) showed obviously odd-even and chain-length dependence.[21, 26] Solvent-responsive 2D morphologies of F−OC_{13} were obtained resulting from the solvent–molecule interactions.[21] However, only F−OC_{13} displaying multiple phases at the aliphatic solvent/graphite interface was investigated. In addition, the nature of such phenomenon was not explained in detail. This prompted us to carry out a systematic study on the self-assembly of F−OC_n with various lengths of alkyl chain units at the *n*-tetradecane and *n*-tridecane/graphite interfaces, respectively.

In this work, we investigate the self-assembly of F−OC_n with different alkoxy chains in length at the aliphatic solvent/graphite interface with various solution concentrations. We will discuss the importance of steric matching and solution concentration to account for the versatility of the supramolecular structures that depend on the chain length of the molecules. STM reveals that the solvent exerts as not only a dispersant but a counterpart participating in the self-assembly formation and results in new structures. Due to the dipolar interactions between the fluorenone cores, there is space between the alkoxy chains of F−OC_n such that the aliphatic solvent molecules are filled further apart. The

stability of these coadsorbed patterns has been ascribed to the perfect interdigitation between the peripheral alkyl chains of F−OC_n and solvent upon self-assembly, which in turn is related to the distance between alkoxy chains attached to the fluorenone moiety. The self-assembled monolayers of F−OC_n (n = 12−16) evolve from a low-density coadsorbed linear lamellar pattern which is formed at low concentrations to high-density patterns at relatively high concentrations. We find that when the alkoxy chain length of F−OC_n is close to that of solvents, the molecular arrangement is easier to exhibit the structural diversity. The results could provide detailed insight into the polymorphism phenomenon exhibited by the molecule−solvent interactions due to steric and concentration effects.

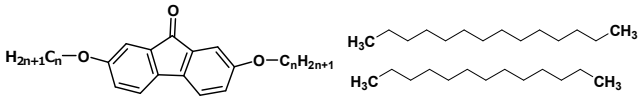

Scheme 1. Chemical structures of 2,7-bis(*n*-alkoxy)-9-fluorenone (F−OC_n, *n* = 12−18) and aliphatic solvents.

2. Experimental Section

2,7-Bis(*n*-alkoxy)-9-fluorenone (F−OC_n, *n* = 12−18) used in this study were synthesized as described in the literatures.[27-28] F−OC_n was obtained by repeated recrystallization in order to ensure the purity. *n*-Tetradecane and *n*-tridecane (TCI) were used as received. The samples were prepared by dropping a droplet (~ 1 μL) of solution that contained F−OC_n (concentration: 10^{-4}~ 10^{-6} mol L^{-1}) onto a freshly cleaved atomically flat surface of HOPG (quality ZYB, Bruker, USA). Most images obtained at the liquid/solid interface were recorded within 2 h after dropping a solution of the F−OC_n. In order to investigate the solvent-dependent, the samples after replaced 2−4 h or longer time were rescanned by STM.

STM measurements were performed on a Nanoscope IIIa Multimode SPM (Bruker, USA) at ambient conditions with the tip immersed in the supernatant liquid. The tips were mechanically cut from Pt/Ir wires (80/20). All the images were recorded with the constant current mode and are shown without further processing. The tunneling parameters are given in the corresponding figure caption. Different tips and samples were used to check the reproducibility and to exclude image artifact that were caused by the tips or the samples. The HOPG lattice was used as an internal standard to correct each STM images and to determine the average lattice parameters of the F−OC_n monolayer by examining at least 4 images.

Molecular models of the assembled structures were built by Materials Studio 4.4. The model of monolayer was constructed by placing the molecules according to the intermolecular distances and angles that were obtained from the analysis of STM images. Semiempirically caculated spatial distribution of the HOMO for F−OC_n is performed by Gaussion 03W. The dipole moment and energy of F−OC_{14} and aggregation were calculated using DFT provided by Dmol3 code with Materials Studio 5.0 software.

3. Results

STM investigation for the self-assembled patterns of F−OC_n was performed at the *n*-tetradecane/graphite interface and *n*-tridecane/graphite interface, respectively. *n*-Tetradecane and *n*-tridecane were selected as solvents because they not only fulfill the technical requirements (less volatile, non-conductive and less affinity for the HOPG surface), but also participate in the self-assembly formation and result in new structures. In all images, regions covered with fluorenone backbones and alkyl chains are observed with high and low tunneling current, which are encoded in bright and dark colors, respectively.[29] All of the fluorenone cores in the STM images are flat on the HOPG surface according to the distribution of electronic state.

With the exception of F−OC_{17} and F−OC_{18}, at low solution concentrations, all compounds F−OC_n could self-assembly into a coadsorbed linear structure at the *n*-tetradecane/graphite interface or *n*-tridecane/graphite interface, in which the alkyl chains in adjacent lamellae arrange in a tail-to-tail fashion. With the change of solution concentration, the self-assembled monolayers of F−OC_{14} exhibit the most complex structural diversity.

3.1 Self-assembled structure of F−OC_{14}

Figure 1 shows the STM images of a coadsorbed linear pattern formed by F−OC_{14} at the tetradecane/HOPG interface under low concentrations (1.3 × 10^{-6} to 5.0 × 10^{-7} mol L^{-1}). Almost the whole scanning area was covered by the equal distant bright lines (Figure 1a). The structural details revealed by a high-resolution STM image (Figure 1b) shows that the linear phase consists of trimeric molecules (blue ellipsoid) arranged in a columnar fashion. The unit cell of F−OC_{14} in the linear phase contains three molecules, which is identified in comparison to the self-assembled pattern of F-OC_{odd} in octanonic acid.[26] The orientation of fluorenone groups can be identified by the HOMO level (Figure 1c).[28] A careful observation reveals that the side chains of one F−OC_{14} molecule are parallel to the fluorenone moieties indicated by a blue arrow in Figure 1b. The fluorenone moieties in other two molecules incline toward the side chains. The fluorenone moieties pack in a linear sequence in each lamella, and the side chains in adjacent lamellea are stacked by a tail-to-tail fashion. By counting the number of the chains and the side chain of F−OC_{14}, we find that the *n*-tetradecane molecules

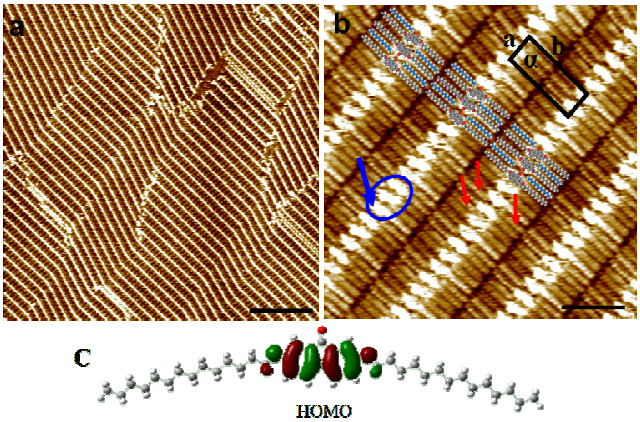

Figure 1. (a, b) Large-scale and high-resolution STM images of F−OC_{14} self-assembled adlayer in tetradecane (1.3 × 10^{-6} mol L^{-1}) on HOPG surface. V_{bias} = 701 mV, I_t = 598 pA. (a) Scale bar = 40 nm; (b) scale bar = 3 nm. The computed structural model is superimposed on the high-resolution STM image. (c) Semiempirically caculated charge density contours of the HOMO for F−OC_{14} by Gaussion 03W.

coadsorb on the HOPG surface (Figure S1, in the ESI†).[24] The molecular model superimposed on the high-resolution STM image reveals that the tetradecane molecules indicated by blue color occupy the space in a loosely-packed assembly and have chance to participate in the assembly formation, resulting from the steric matching. The interdigitated solvent molecules could be observed clearly as the red arrows indicated in Figure 1b. The insertion of solvent molecules in the 2D crystalline lattice leads to a linear structure, which is similar to a previous report for the self-assembly of F−OC_{13}.[21]

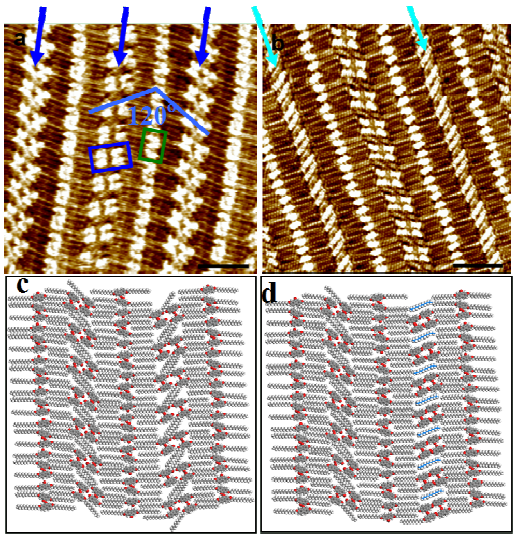

Figure 2. (a, b) High-resolution STM images of F−OC_{14} self-assembled monolayer in tetradecane (2.5×10^{-4} mol L^{-1}) on HOPG surface showing two kinds of alternated patterns. V_{bias} = 650 mV, I_t = 500 pA. Scale bar = 4 nm. (c, d) Molecular models illustrating the self-assembly patterns based on the STM images.

At high concentrations (7.5×10^{-4} mol L^{-1} to 1.0×10^{-4} mol L^{-1}), an alternate phase appeared in the self-assembled adlayer of F−OC_{14} on the HOPG surface (Figure S2a, in the ESI†). The domain size for the alternate pattern is relatively small (10−15 domains per 200 nm^2 area). Increasing the concentration is expected to enhance the number of nucleation sites thus leading to small domains. Through careful observation, we found that two kinds of alternate structures were formed as shown in Figure 2 and S2b. In Figure 2a, the trimeric (green rectangle) and tetrameric (blue rectangle) bright lines appear alternately. The arrangement of trimeric line is similar to the linear pattern in Figure 1. In the tetrameric line (blue arrows), each lamella consists of two molecular rows. In one row, two molecules form a dimer with a back-to-back configuration and arrange with adjacent dimer in another row with a head-to-head fashion. The packed orientation of the tetramers in adjacent tetrameric lines is different and the angle between them is 120 ± 2º as indicated in Figure 2a. A structural model based on the STM image shows that two alkyl chains for two molecules in the tetramer are not adsorbed on the HOPG surface, thus back-folded in the supernatant solution, as previously described for other systems exposing alkoxy side-chains.[30-32]

Another alternate pattern is shown in Figure 2b. Unlike the pattern in Figure 2a, the lamellae indicated by green arrows apparently consist of bright and dark rods. The brighter rod displays eight lobes per two fluorenone groups, which corresponds to charge density contours of HOMO level. Such feature can not be observed for the darker rod. Owing to the high tunneling current, in each lamella two neighboring brighter rods (about 1.8 nm in length) should be the conjugated fluorenone moieties, which is slightly longer and wider than the tetradecane molecule (about 1.6 nm in length). Only the F−OC_{14} and tetradecane molecule exist in the experimental system, so we conclude that a solvent molecule in the gap between two brighter fluorenone groups. The darker rod is the coadsorbed tetradecane molecule, which is not clearly observed in most STM images (Figure S2b, in the ESI†). In Figure 2, the brighter alkyl chains appear due to the mismatch with HOPG lattices. We propose the molecular packing model in Figure 2d. For the lamellae as indicated by green arrows in Figure 2b, four F−OC_{14} molecules arrange in a densely head-to-head fashion resulting in one side chain of F−OC_{14} desorbs from the HOPG surface. The space between the tetramers is filled by the tetradecane molecules, which are shown in Figure 2d as the blue alkyl chains.

The alternated patterns with high density (Figure 2) are formed from relatively concentrated solutions of F−OC_{14} and are the most stable structures over a wide concentration range (7.5×10^{-4} mol L^{-1} to 1.0×10^{-4} mol L^{-1}). While they are the sole morphologies observed at higher concentrations and coexist with the coadsorbed linear structure observed at low concentrations (Figure S3, in the ESI†). Systematic concentration dependent experiments reveal that there is considerable overlap in the concentration, over which the linear and alternate patterns are stable.

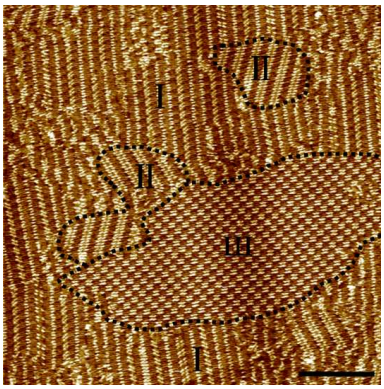

Figure 3. A typical STM image of the F−OC_{14} self-assembled monolayer in tetradecane (7.5×10^{-4} mol L^{-1}) on HOPG surface showing the coexistence of three kinds of assembled patterns after the sample was placed more than 5 hours. V_{bias} = 610 mV, I_t = 520 pA. Scale bar = 40 nm.

At higher concentrations range of 1.5×10^{-4} mol L^{-1} to 5.6×10^{-3} mol L^{-1}, a less ordered pattern without obvious domain boundary was obtained (Figure S4, in the ESI†), which further indicates that the number of nucleation sites is associated with the concentration. However, after the sample was placed more than 5 h, the molecular arrangement in order enhanced and the coexistence of three stable phases was observed as shown in Figure 3, which are labeled as structure I, II and III. During the scanning for each pattern, no obvious structural transition among them was found. However, the large scale STM images (Figure S5, in the ESI†) obtained in different regions show that the total area of ordered structure I, II and III became larger with the

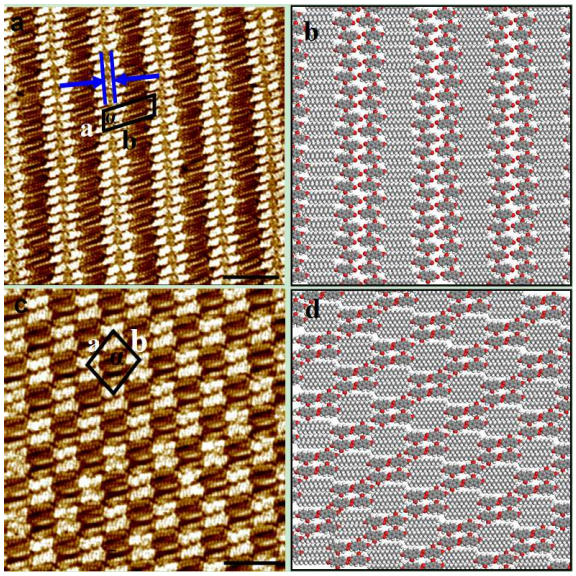

Figure 4. (a) High-resolution STM image of structure II for F−OC_{14}. V_{bias} = 650 mV, I_t = 480 pA. (b) Proposed assembly model for structure II. Scale bar = 4 nm. (c) High-resolution STM image of structure III for F−OC_{14}. V_{bias} = 648 mV, I_t = 530 pA. Scale bar = 4 nm. (b) Proposed assembly model for structure III.

extension of the scanning time. Two new structures (structure II and III) with densely packed molecules appear. This reflects the sensitivity of the system towards changes in the concentration due to the solvent evaporation. Since the STM experiments are performed in an open chamber, the evaporation of tetradecane is unavoidable thus leading to a concomitant rise in the concentration.

From the high-resolution image of structure II (Figure 4a), one may identify a two-row linear arrangement, in which two adjacent fluorenone cores (left and right) pack head-to-head with an inverse direction by reference to the carbonyl group. The larger distance between the fluorenone cores in each two-row line indicated by blue arrows is 0.67 ± 0.03 nm. The structural model shown in Figure 4b illustrates that one side chain of F−OC_{14} desorbs from the HOPG surface by counting the number of the chains and the side chain of F−OC_{14}, while the other side chain arranges interdigitally, due to the space constraint. The desorbed side chains are above the monolayer, and then they are seen as 'high points' between the conjugated moieties in the STM image. The structural unit of this phase is defined by the rhomboid in Figure 4a with a = 1.5 ± 0.1 nm, b = 3.8 ± 0.2 nm, and α = 75 ± 1° and the unit area is 5.5 nm^2. The packing density of F−OC_{14} molecules is about 0.73/nm^2, higher than those of coadsorbed and alternate phases.

Another pattern with high density is shown in Figure 4c. The π-conjugated units and alkyl chains are alternately aligned in a zigzag mode. The length of each bright rod is 1.9 ± 0.1 nm, which corresponds to the length of two fluorenone groups. According to the proposed model in Figure 4d, two fluorenone cores arrange in a compact head-to-head fashion with an inverse direction by reference to the carbonyl group. We propose that such pattern is formed resulting from the length matching of the side chains and the conjugated moieties, which is not observed in the self-assembly of other molecules. The unit parameters are a = 2.7 ± 0.1 nm, b= 3.2 ± 0.2 nm, and α = 74 ± 2°. The unit area is 5.5 nm^2, which is the same with structure II. Although structure III is obvious different from structure II, the molecule−molecule and molecule−substrate interactions are the same. The chain desorbed phenomenon only happens under high concentrations. The high molecular density in solution results in the high density of molecular adsorption. This decreases both the adsorbate-adsorbate and adsorbate-substrate interactions at the level of single molecule. Moreover, due to the intermolecular dipolar interactions, the dislocated inverse arrangement of cores makes the system reach the lowest energy. So the dense packed structures are mainly determined by the dipolar interaction between the fluorenone cores, rather than the interaction involving the alkyl groups.

The coadsorbed linear pattern was also observed for the self-assembly of F−OC_{14} at the tridecane/HOPG interface under low concentrations (Figure S6a, in the ESI†). At high concentrations, the similar alternate patterns were formed (Supporting Information, Figure S6b-c). After the sample with a high concentration was placed over 12 h, the whole area was covered by the alternate patterns (Figure S7, in the ESI†) and no densely packed patterns were found. Since the length of tridecane is slightly shorter than the alcoxyl chain of F−OC_{14}, the van der Waals interaction between them decreases significantly with the evaporation of solvent. Thus, under low concentrations, after the sample was placed over 12 h, another linear phase consisting of dimers was formed as shown in Figure 5a, which is not observed in tetradecane. Two molecules form a dimer in a back-to-pack fashion. The adjacent dimers in each lamella pack with a dislocated arrangement (Figure 5b). Molecular model of the zigzag structure based on the STM image is proposed in Figure 5c. The unit cell can be defined with a = 2.2 ± 0.1 nm, b= 3.5 ± 0.2 nm, and α = 53 ± 2°. The molecular density is 0.49/nm^2, which is obviously lower than structure II and III.

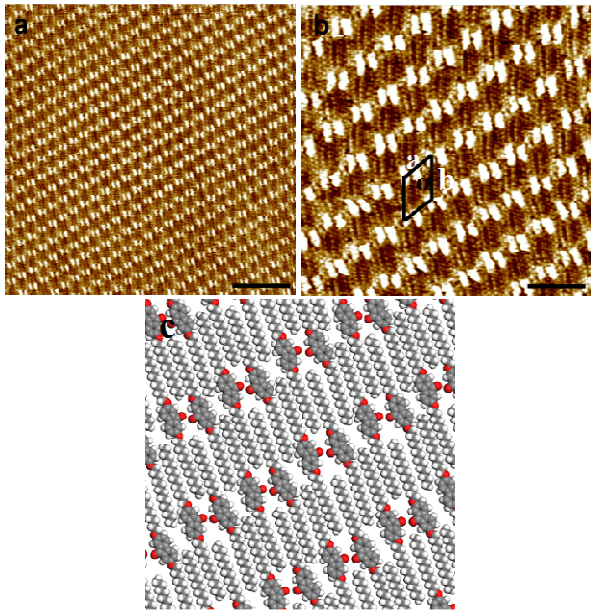

Figure 5. (a, b) Large-scale and high-resolution STM images of F−OC_{14} self-assembled monolayer in tridecane with a low concentration (3.5×10^{-6} mol L^{-1}) on HOPG surface after the sample was placed more than 12 hours. V_{bias} = 630 mV, I_t = 505 pA. (a) Scale bar = 10 nm; (b) scale bar = 4 nm. (c) Molecular model of the zigzag structure based on the STM image.

3.2 Self-assembled structure of F−OC$_n$ (n = 12, 15−18)

Other F−OC$_n$ molecules showed the similar 2D linear coadsorbed pattern at the *n*-tetradecane or *n*-tridecane/graphite interfaces under low concentrations except for F−OC$_{17}$ and F−OC$_{18}$. For F−OC$_{12}$, at low concentrations, the stable assembled adlayer displaying the coadsorbed lamella pattern could be observed at the tridecane/HOPG interface as shown in Figure 6a. The molecular model is proposed in Figure 6b. Although such pattern was also formed at the tetradecane /HOPG interface (Supporting Information, Figure S8a), the adlyer was not stable enough so that the high-resolution image could not be obtained easily. After the sample was scanned over 5 h, the zigzag linear pattern also appeared (Figure S8b, in the ESI†). In the previous work, we found that F−OC$_{12}$ could only adsorb on the HOPG surface and form a pliers-like structure using 1-phenyloctane as the solvent. In 1-octanoic acid, 1-octanol and dichloromethane, no adlayer was observed.[26] The results indicate that solvent coadsorption could enhance the stability of the monolayer and F−OC$_{12}$ tends to adsorb on HOPG surface in nonpolar solvents.

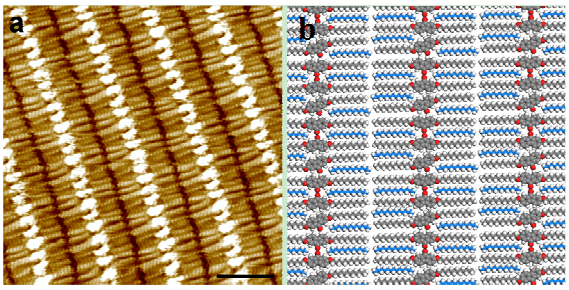

Figure 6. (a) High-resolution STM image of F−OC$_{12}$ self-assembled monolayer in tridecane on HOPG surface under low concentrations. V_{bias} = 630 mV, I_t = 520 pA. Scale bar = 4 nm. (b) Molecular model of the coadsorbed linear structure based on the STM image.

For F−OC$_{15}$, after the solution was dropped on the HOPG surface, the coadsorbed linear phase was obtained (Figure S9a, in the ESI†) at the tridecane/HOPG interface under low concentrations. While the sample was scanned for about 1 h, a new linear pattern was observed (Figure 7a). The structural details are revealed by a high-resolution STM image shown in Figure 7b. In each lamella, the fluorenone cores displaying the bright dots arrange densely with the same direction. The conjugated moieties in adjacent lamellae pack in an opposite orientation. The arrangement of alkyl chains on both sides of the conjugated groups is different completely. On the left side, all the alkyl chains pack in the same direction along the graphite lattice as one blue arrow indicated in Figure 7b. However, on the right side, the alkyl chains connecting with the fluorenone groups pack densely. Moreover, the right stripes in adjacent lamellae arrange in different directions. The orientation of alkyl chains as the other blue arrow indicated in Figure 7b corresponds to the 3-fold of graphite lattice. While a third type of side chains is forming angle of 45º with respect to the lamlellar axis. In addition, a careful observation reveals that the alkyl chains arrange in two kinds of orientations. The alkyl chains connecting with the fluorenone group is lying perfectly flat on the HOPG surface. While the coadsorbed tridecane indicated by blue color in Figure 7c shows a thinner line, which undergo orientation adjustment by titling or rolling involving the rotation of the molecular backbone relative to the substrate due to the space limit.[33]

On the basis of STM observation, a structural model for the new lamellar pattern is proposed in Figure 7c. The results also identify the sensitivity of the system towards changes in the concentration due to the solvent evaporation. The evaporation of tetradecane causes part adsorbed solvent molecules to desorb from the HOPG surface. In order to keep the densely packing, the arrangement of fluorenone groups becomes more orderly. The result indicates that the greater difference in length between the side chain and solvent, the less stable of the coadsorbed linear pattern.

After the above sample was placed in ambient conditions for 3 h, the whole scanning area was covered only by a linear structure consisting of trimers. (Figure S10a, in the ESI†), which is the same with the self-assembly of F−OC$_{15}$ in phenyloctane.[26] No zigzag pattern was observed. Using the tridecane or tetradecane as the solvent, at high concentrations, the linear patterns were also observed (Figure S10b−c, in the ESI†). At the tetradecane/HOPG interface under low concentrations, the coadsorbed lamellar pattern is formed, which is more stable than that at tridecane/HOPG interface due to the stronger molecule−solvent interactions (Figure S9b, in the ESI†).

For F−OC$_{16}$, after the solution with a low concentration was dropped on the HOPG surface, the coadsorbed linear pattern could be observed at the tetradecane/HOPG interface (Figure S9c, in the ESI†). However, as the extension of scanning time, the linear pattern could transform into alternate and zigzag patterns as shown in Figure 8a. Finally, the whole scanning area was covered by the zigzag structure (Figure S11, in the ESI†). The alternate pattern is the same with the self-assembly of F−OC$_{16}$ in phenyloctane.[26] The high-resolution STM image as shown in Figure 8b reveals the molecular packing details of zigzag pattern. Two molecules form a dimer in a back-to-pack fashion. The adjacent dimers in a lamella pack with a dislocated arrangement. The molecular model is proposed in Figure 8c.

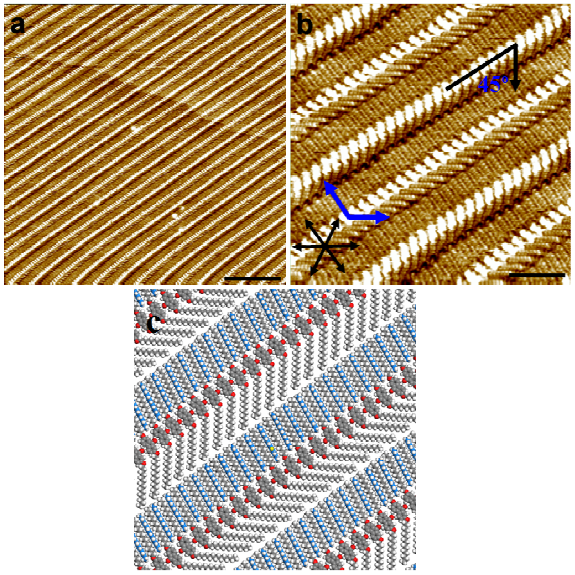

Figure 7. (a, b) Large-scale and high-resolution STM images of F−OC$_{15}$ self-assembled monolayer in tridecane on HOPG surface under a low concentration, after the sample was scanned for about 1 h. V_{bias} = 630 mV, I_t = 520 pA. (a) Scale bar = 20 nm; (b) scale bar = 4 nm. (c) Molecular model of the linear structure based on the STM image.

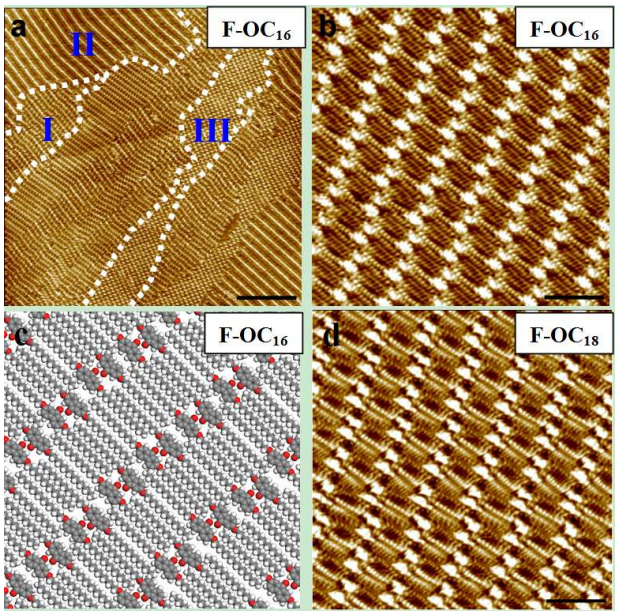

Figure 8. (a) Large-scale STM image of F−OC_{16} self-assembled monolayer in tetradecane on HOPG surface under low concentrations. Scale bar = 40 nm. (b) High-resolution STM image of F−OC_{16} showing the arrangement of zigzag pattern V_{bias} = 640 mV, I_t = 520 pA. Scale bar = 4 nm. (c) Molecular model of the zigzag structure based on the STM image of F−OC_{16}. (d) High-resolution STM image of F−OC_{18} self-assembled monolayer in tetradecane on HOPG surface. V_{bias} = 640 mV, I_t = 520 pA. Scale bar = 4 nm.

At the tridecane/HOPG interface, the alternate and zigzag patterns of F−OC_{16} were obtained under low concentrations (Figure S12, in the ESI†). Under high concentrations, only the zigzag phase exists at the tetradecane/ HOPG interface and tridecane/HOPG interface, respectively. No coadsorbed pattern was obtained.

When the tetradecane and tridecane were used as the solvents, no self-assembled structure for F−OC_{17} was observed. However, in 1-phenyloctane and 1-octanoic acid, the trimeric linear pattern was formed. In addition, at the gas/HOPG interface, only F−OC_{17} formed a zigzag pattern with tetramer.[26] The results indicate that F−OC_{17} molecules incline to form adlayers in polar solvents. Furthermore, it maybe result from its special thermodynamic property characterized by DSC.[26] Up till now, the reason of these special results can not be explained distinctly. Thus, we leave this for future study. For F−OC_{18}, at low concentrations using tetradecane and tridecane as the solvents, only the zigzag pattern was obtained as shown in Figure 8d.

The formation of the coadsorbed lamellar pattern present in the assembly of F−OC_n is essentially the same as it is determined by the length of alkoxy chains. Owing to the lengthening of the alkoxy side chain, the van der Waals interactions of molecule−molecule and molecule−substrate become stronger. However, the difference in length between the side chain of F−OC_n (n = 16−18) and the alkoxy chain of solvent become bigger resulting in the mismatching of alkyl chains, furthermore decreasing the molecule−solvent interactions. Thus, when the side chain number of F−OC_n (*n*) is more than 15, the coadsorbed lamellar pattern is not stable enough to be observed, even is not formed on the HOPG surface. The zigzag pattern is the most stable architecture considering the total gain in the energy of the system based on higher surface density of adsorbed molecules.

4. Discussion

Table 1 and Table S1 summarizes the geometric characteristics, adsorption structures, unit cell parameters and plane group of the 2D self-assembled patterns of physisorbed adlayers observed in 2D assembly of F−OC_n at tetradecane and tridecane/HOPG interface under different concentrations. For F−OC_n (n = 12−16), the coadsorbed lamellar pattern is formed. For the F−OC_n molecules with odd number of carbon atom in the side chain (n = 13, 15, 17), the zigzag structure is not observed.

The self-assembly of F−OC_n at the aliphatic solvent/graphite interface is obvious different from that at the phenyloctane/graphite interface. Solvent−molecule interactions might play an important role in the self-assembly of F−OC_n. At ambient conditions, the solvent is difficult to form stable monolayer on the HOPG surface. In this system, we propose that the self-assembled variety of F−OC_n is associated with the solvent coadsorption and solvent polarity.

4.1 Effect of coadsorption

At the liquid/solid interface, there is an equilibrium between the molecules (or coadsorbed solvent) adsorbed on the surface and those which go back into the solution.[34-35] If the solvent contains alkyl chain, aromatic ring, and hydrogen bonding donors or acceptor, the solvent could be coadsorbed at the liquid/solid interface via space matching, van der Waals interactions or hydrogen bonding with the adsorbates. In addition, the molecule tends to arrange with a densely packing pattern.[36] For the self-assembly of F−OC_n, solvent coadsorption could induce the formation of denser monolayer. In previous study we have found that F−OC_{13} showed concentration dependent in phenyloctane.[21] With the decreasing of the solution concentration, more and more phenyloctane molecules filled the voids resulting in the appearance of new patterns. The solvent coadsorption could improve the stability of the supramolecular assembled structure, especially allowing for the construction of 2D multicomponent self-assembled architectures and also immobilizing and imaging of small solute molecules that can not be imaged in monomolecular adlayers owing to their high mobility.[37-38]

Due to the polarity of the fluorenone cores, the F−OC_n molecule tends to arrangement in different orientations in order to get the lowest energy.[26] At the *n*-tridecane or *n*-tetradecane/HOPG interface under low concentrations, to maximize the substrate coverage, which is favored for enthalpic reasons, fluorenone cores could form trimers and arrange more densely. So the *n*-tridecane or *n*-tetradecane molecules coadsorb on the side chain lamella due to the space effect, giving rise to a closely packed structure and favorable van der Waals interactions between the alkyl chains. This observation is interpreted from geometric considerations, in which the *n*-tridecane or *n*-tetradecane molecule could fit into the voids left by the side chains of the F−OC_n molecule. The original space of interdigitated side chains of F−OC_n is replaced by the solvent molecules. The closer the chain length of F−OC_n is to that of solvent, the stronger the van der Waals interactions between the molecule and solvent are and the more stable the coadsorbed lamella is. For the molecules with alkyl side chains, the

interdigitated chain is energetically favored, while for the systems that have both adsorbate and solvent chain−chain interactions, the coadsorption decreases the van der Waals interactions of molecule−molecule due to the decreased density of CH_2 units upon replacement of the F−OC_n side chain with solvent molecules. The side chains of F−OC_n in adjacent lamellae arrange by a tail-to-tail configuration instead of interdigitally, indicating that the van der Waals interactions between the side chain and the coadsorbed solvent molecule enhance the stability of the adlayer.

Table 1. Schematic Representation and Unit Cell Parameters of all Phases Observed in 2D Self-Assembly Monolayers of F−OC_n at Tetradecane and Tridecane/HOPG Interfaces under Different Concentrations

F-OC_n	Solvent	Structure model	Concentration (mol L^{-1})	a (nm)	b (nm)	α (°)	Density, S (nm^2 per molecule)	Plane group
n = 12	tetradecane	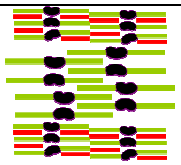	$<10^{-6}$	1.6 ± 0.1	4.6 ± 0.2	90	2.45	*P1*
			$>10^{-4}$ ~saturated	2.2 ± 0.1	3.3 ± 0.2	70 ± 1	0.91	*P1*
	tridecane		$<10^{-6}$	1.6 ± 0.1	4.5 ± 0.1	90	2.40	*P1*
n = 13*	tetradecane	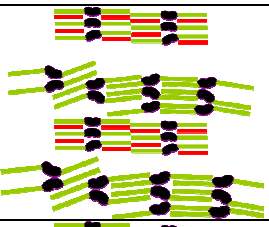	$<10^{-6}$	1.6 ± 0.1	4.2 ± 0.1	90	2.24	*P1*
			$\sim10^{-5}$	–	–	–	–	–
	tridecane		$<10^{-6}$	1.6 ± 0.1	4.2 ± 0.1	90	2.24	*P1*
			$\sim10^{-5}$	–	–	–	–	–
n = 14	tetradecane	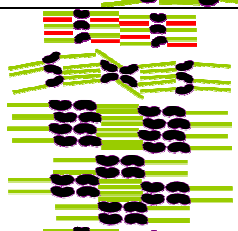	$<10^{-6}$	1.6 ± 0.1	4.9 ± 0.1	90	2.61	*P1*
				–	–	–	–	–
			$\sim10^{-5}$	1.5 ± 0.1	3.8 ± 0.2	75 ± 1	0.73	*P1*
				2.7 ± 0.1	3.2 ± 0.2	74 ± 2	0.73.	*P2*
	tridecane	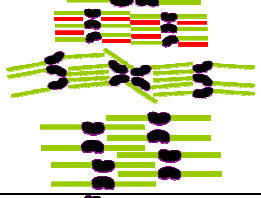	$<10^{-6}$	1.6 ± 0.1	4.9 ± 0.1	90	2.61	*P1*
			$\sim10^{-5}$	–	–	–	–	–
			$>10^{-4}$ ~saturated	2.2 ± 0.1	3.5 ± 0.2	53 ± 2	0.49	*P1*
n = 15	tetradecane	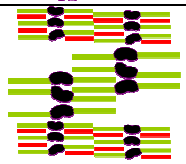	$<10^{-6}$	1.6 ± 0.1	5.0 ± 0.1	90	2.67	
			$>10^{-4}$ ~saturated	1.6 ± 0.1	2.9± 0.1	70 ± 1	0.59	*P1*
	tridecane		$<10^{-6}$	1.6 ± 0.1	5.0 ± 0.1	90	2.67	
			$\sim10^{-5}$	–	–	–	–	–
n = 16	tetradecane	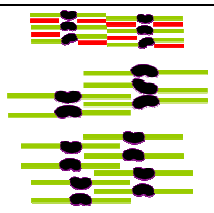	$<10^{-6}$	1.6 ± 0.1	5.1 ± 0.1	90	2.72	*P1*
			$\sim10^{-5}$	2.1 ± 0.1	5.8 ± 0.2	90	2.90	–
				2.2 ± 0.1	3.7 ± 0.1	75 ± 1	1.10	*P1*
	tridecane		$<10^{-6}$	2.1 ± 0.1	5.8 ± 0.2	90	2.90	–
			$>10^{-4}$ ~saturated	2.2 ± 0.1	3.7 ± 0.1	75 ± 2	1.10	*P1*
n = 18	tetradecane		$>10^{-4}$ ~saturated	2.2 ± 0.1	3.8 ± 0.1	67 ± 1	1.01	*P1*

* The data were presented according to previous results in reference 21. - The cell parameters are not determined due to the irregular arrangement.

For F−OC_n (n = 13, 14), the length of the side chain is close to that of solvent molecule. The coadsorbed linear structure is stable. While for F−OC_n (n = 12, 15−16), the greater the length between the side chain and solvent molecule is different, the worse the stability of the coadsorbed linear structure is. Even, no coadsorption happens for F−OC_n (n = 17−18).

4.2 Effect of solvent polarity and intermolecular dipole−dipole interactions

For the solvent-induced polymorphism without solvent coadsorption, the solvent effect is more important in tuning the molecular structure only by changing the environment of adsorbates. Clearly, the nature of solvent must play a key role. The polarity of the solvents is the most crucial factor that affects the molecular assembly for the molecules with polar functional groups. When the solvent was evaporated completely or the nonpolar molecule acts as the solvent (no coadsorption), the molecule−solvent interactions are inexistence or very weak. In our system, the solvent participate in the coadsorption, so the molecule−solvent interactions are enhanced. A balance between intermolecular van der Waals interactions of side chains and the dipole−dipole interactions of fluorenone groups mainly dominates the molecular self-assembled pattern.

The F−OC_n has relative stronger polarity, which is easier to dissolve in polar solvents. If the molecule−substrate interactions are not strong enough, the molecule could not adsorb on the HOPG surface. So F−OC_{12} only forms a monolayer in the nonpolar solvents (phenyloctane[26] and aliphatic solvent). Under high concentrations, with the lengthening of the side chain of F−OC_n, the molecule−molecule and molecule−substrate interactions increase gradually. Thus, except for F−OC_n (n = 13, 15, 17), all the molecules are more likely to form the densely zigzag pattern with the higher molecular density in the adlayers of F−OC_n. Two molecules arranged in the back-to-back fashion eliminate the intermolecular dipolar interactions. In addition, the zigzag pattern was only observed in nonpolar solvents.

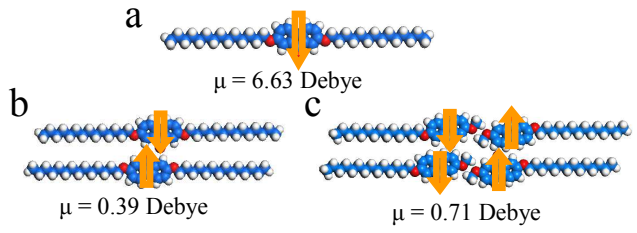

Figure 9. (a) Dipole moment (μ) of free F-OC_{14} based on the molecular conformation. (b) Dipole moment of the optimized dislocated dimer in the zigzag pattern of F-OC_{14}. (c) Dipole moment of the optimized tetramer for the self-assembly patterns of F-OC_{14} under high concentrations.

In order to interpret the intermolecular dipolar interactions, we take the F−OC_{14} as an example. Figure 9 shows the theoretical caculated dipole moment for different patterns of F−OC_{14}. The dipole moment of free F−OC_{14} with single molecular conformation as shown in Figure 9a is calculated to be μ = 6.63 D. Generally, the molecular dipoles tend to arrange in collinear or antiparallel modes to maximize the dipole−dipole interaction, as is schematically shown in Figure 9b and c. We found experimentally that the F−OC_n (n = 12, 14, 16, 18) molecules can form the paired arrangement with the dislocated antiparallel fashion of fluorenone units (Figure 9b), because changing the length of side chain does not alter the intermolecular dipole−dipole interactions along the lamellar direction. The antiparallel arrangement of molecular dipole of fluorenone units (Figure 9b-c) could avoid potential dipole repulsions. The dipole moment of the dislocated antiparallel pattern is decreased to be 0.39 D. The calculated dipole moment of the tetramer is 0.71 D, which is also less than that of the free molecule obviously. The results reveal that the the intermolecular dipole−dipole interactions contribute to the molecular arrangement.

4.3 Effect of chain-length and concentration

Changing the side chain length of F−OC_n, the self-assembled structures show obvious difference. The results indicate the self-assembly of F−OC_n exists chain-length dependence. At low concentrations, except for F−OC_{17} and F−OC_{18}, the coadsorbed linear pattern was observed. However, with the lengthening of the side chain, the stability of the monolayer becomes lower. Apparently, if the length of the coadsorbed solvent molecules is shorter than the length of the F−OC_n side chains significantly, the van der Waal interactions between the side chain and solvent are not strong enough to keep the coadsorbed monolayer stable resulting from the weaker steric matching.

A question arises as to why only F−OC_{14} exhibits complex structural variety. The 2D self-assembled structures of F−OC_n on HOPG surface are determined by four possible driving forces: (i) chain−HOPG lattice interactions (molecule−substrate interactions); (ii) van der Waals interactions between the alkyl chains (molecule−molecule interactions); (iii) dipole−dipole interactions between the fluorenone cores (molecule−molecule interactions); (iv) fluorenone derivative−solvent interactions (molecule−solvent interactions). Molecular self-assembly for F−OC_n at the surface in liquid conditions is a balance of the above four kinds of interactions. As the alkyl chain length is decreased, both the alkyl−graphite interactions and the van der Waals interactions between the alkyl chains decrease. The dipole−dipole interactions between the fluorenone cores and molecule−solvent interactions (no coadsorption) remain invariable. So, for F−OC_{14} under high concentrations the molecule−molecule interactions are relatively enhanced. In addition, the length of the side chain for F−OC_{14} is almost equal to that of tetradecane, which results in well space matching and maximized molecule−solvent van der Waals interactions. After some solvent evaporates, even one side chain of F−OC_{14} desorbs from the HOPG surface in order to reach the highest molecular density, although the tetradecane does not coadsorb on the surface.

The assembly process is dynamic and controlled by the adsorption–desorption equilibrium.[32] It is generally acknowledged that the adsorption–desorption process was under thermodynamic control. The adsorption−desorption equilibrium determined the surface coverage ratio of different structures. The concentration dependency of the self-assembly of F−OC_n can therefore be understood as resulting from the different stabilities and molecular densities of different polymorphs. In general, the driving force for the molecular assembly is related to the minimization of Gibbs free energy which is composed of an enthalpic gain and entropic loss. The enthalpic gain results from

attractive adsorbate–adsorbate and adsorbate–substrate interactions, while the entropy is generally weaken when molecules associate or adsorb on a surface. The different energy among different polymorphs determines the system sensitivity towards concentration: the larger the energy difference, the more dramatic the concentration dependence. Our system is relatively complex, because the effect factor of coadsorption has to be considered. Attempts to follow the recently published thermodynamic method remained futile, no concentration and solvent coadsorption among the coverage of different structures according to the proposed formalism was found.[10, 39-40] Thus, our results could display a general observed trend for concentration induced self-assembled polymorphism at the aliphatic solvent/HOPG interface: higher solution concentration lead to more densely packed arrangement.

5. Conclusion

Structural polymorphism in 2D self-assembled adlayers evokes careful attention, because processing conditions such as concentrations of building blocks and the choice of solvent can significantly affect the nanoscale structure of the monolayers. This study expounds the concentration controlled structural variety in self-assembled monolayers of a series of fluorenone derivatives. By choosing the solution concentration, it is possible to control the nanostructure formed on HOPG surface. Lower concentrations favored the formation of coadsorbed lamellar pattern due to steric matching, whereas the high concentrations led to the formation of a densely packed zigzag pattern. F−OC_{14} exhibited complex structural variety, in which a systematic trend of decrease in the molecular density per unit cell with decreasing concentration was obtained. The closer the length of the side chain for F−OC_n is to that of tetradecane or tridecane, the more stable coadsorbed pattern is formed, which results in well space matching and the maximized van der Waals interactions between molecule and solvent.

Acknowledgements

Financial supports from the National Program on Key Basic Research Project (2012CB932900), the National Natural Science Foundation of China (21103053, 51373055) and the Fundamental Research Funds for the Central Universities (SCUT) are gratefully acknowledged.

Notes and references

College of Materials Science and Engineering, South China University of Technology, Guangzhou 510640, China. E-mail:msxrmiao@scut.edu.cn, wldeng@scut.edu.cn; Tel: +86 (0) 20 22236708

† Electronic Supplementary Information (ESI) available: Supporting Information Available: Additional STM images of F−OC_n in *n*-tetradecane and *n*-tridecane solvents. See DOI: 10.1039/b000000x/

1 L. Wang, B. J. V. Tongol, S. L. Yau, T. Otsubo, K. Itaya, *Langmuir* 2010, **26**, 7148.

2 S. Klyatskaya, F. Klappenberger, U. Schlickum, D. Kühne, M. Marschall, J. Reichert, R. Decker, W. Krenner, G. Zoppellaro, H. Brune, J. V. Barth, M. Ruben, *Adv. Funct. Mater.* 2011, **21**, 1230.

3 G. M. Florio, K. A. Stiso, J. S. Campanelli, *J. Phys. Chem. C* 2012, **116**, 18160.

4 I. Destoop, E. Ghijsens, K. Katayama, K. Tahara, K. S. Mali, Y. Tobe, S. De Feyter, *J. Am. Chem. Soc.* 2012, **134**, 19568.

5 N. Thi Ngoc Ha, T. G. Gopakumar, M. Hietschold, *J. Phys. Chem. C* 2011, **115**, 21743.

6 M. J. J. Coenen, M. Cremers, D. den Boer, F. J. van den Bruele, T. Khoury, M. Sintic, M. J. Crossley, W. J. P. van Enckevort, B. L. M. Hendriksen, J. A. A. W. Elemans, S. Speller, *Chem. Commun.* 2011, **47,** 9666.

7 R. Gutzler, T. Sirtl, J. F. Dienstmaier, K. Mahata, W. M. Heckl, M. Schmittel, M. Lackinger, *J. Am. Chem. Soc.* 2010, **132**, 5084.

8 C. Marie, F. Silly, L. Tortech, K. Mullen, D. Fichou, *ACS Nano* 2010, **4**, 1288.

9 Z. Mu, O. Rubner, M. Bamler, T. Blömker, G. Kehr, G. Erker, A. Heuer, H. Fuchs, L. Chi, *Langmuir* 2013, **29**, 10737.

10 R. Gutzler, T. Sirtl, J. r. F. Dienstmaier, K. Mahata, W. M. Heckl, M. Schmittel, M. Lackinger, *J. Am. Chem. Soc.* 2010, **132**, 5084.

11 P. M. Zalake, K. George Thomas, *Langmuir* 2013, **29**, 2242.

12 T. Sakano, J.-y. Hasegawa, K. Higashiguchi, K. Matsuda, *Chem. – Asia. J.* 2012, **7,** 394.

13 Y. T. Shen, N. B. Zhu, X. M. Zhang, S. Lei, Z. Wei, M. Li, D. Zhao, Q. D. Zeng, C. Wang, *ChemPhysChem* 2013, **14**, 92.

14 A. V. Aggarwal, S.-S. Jester, S. M. Taheri, S. Förster, S. Höger, *Chem. –Eur. J.* 2013, **19**, 4480.

15 M. O. Blunt, J. C. Russell, M. d. C. Giménez-López, J. P. Garrahan, X. Lin, M. Schröder, N. R. Champness, P. H. Beton, *Science* 2008, **322**, 1077.

16 S. L. Lee, Y. C. Chu, H. J. Wu, C. H. Chen, *Langmuir* 2011, *28*, 382.

17 Y. Liu, G. CuiZhong, Y. Wan, W. JingYi, Y. HuiJuan, Z. Xu, W. ZhaoHui, Z. XiaoWei, L. YuLiang, W. Dong, W. LiJun, *Sci. China–Chem.* 2013, **56**, 124.

18 Y. L. Huang, W. Chen, H. Li, J. Ma, J. Pflaum, A. T. S. Wee, *Small* 2010, **6**, 70.

19 W. Mamdouh, H. Uji-i, J. S. Ladislaw, A. E. Dulcey, V. Percec, F. C. De Schryver, S. De Feyter, *J. Am. Chem. Soc.* 2006, **128**, 317.

20 X. R. Miao, L. Xu, Z. M. Li, W. L. Deng, *J. Phys. Chem. C* 2011, **115**, 3358.

21 L. Xu, X. R. Miao, B. Zha, W. L. Deng, *J. Phys. Chem. C* 2012, **116**, 16014.

22 S. Ahn, A. J. Matzger, *J. Am. Chem. Soc.* 2010, **132**, 11364.

23 T. Chen, D. Wang, X. Zhang, Q. L. Zhou, R. B. Zhang, L. J. Wan, *J. Phys. Chem. C* 2010, **114**, 533.

24 X. Zhang, Q. Chen, G. J. Deng, Q. H. Fan, L. J. Wan, *J. Phys. Chem. C* 2009, **113,** 16193.

25 X. Zhang, T. Chen, Q. Chen, G. J. Deng, Q. H. Fan, L. J. Wan, *Chem.-Eur. J.* 2009, **15**, 9669.

26 L. Xu, X. R. Miao, B. Zha, K. Miao, W. L. Deng, *J. Phys. Chem. C* 2013, **117**, 12707.

27 A. V. Ivanov, S. A. Lyakhov, M. Y. Yarkova, A. I. Galatina, A. V. Mazepa, *Russ. J. Gen. Chem.* 2002, **72**, 1435.

28 L. Xu, X. R.Miao, X. Ying, W. L. Deng, *J. Phys. Chem. C* 2012, **116**, 1061.

29 R. Lazzaroni, A. Calderone, J. L. Bredas, J. P. Rabe, *J. Chem. Phys.* 1997, **107**, 99.

30 Y. Kaneda, M. E. Stawasz, D. L. Sampson, B. A. Parkinson, *Langmuir* 2001, **17**, 6185.

31 Y. Miyake, T. Nagata, H. Tanaka, M. Yamazaki, M. Ohta, R. Kokawa, T. Ogawa, *ACS Nano* 2012, **6**, 3867.

32 S. B. Lei, K. Tahara, F. C. De Schryver, M. Van der Auweraer, Y. Tobe, S. De Feyter, *Angew. Chem. Int. Edit.* 2008, **47**, 2964.

33 D. M. Cyr, B. Venkataraman, G. W. Flynn, *Chem. Mater.* 1996, **8**, 1600.

34 M. Lackinger, S. Griessl, W. A. Heckl, M. Hietschold, G. W. Flynn, *Langmuir* 2005, **21**, 4984.

35 L. Kampschulte, M. Lackinger, A. K. Maier, R. S. K. Kishore, S. Griessl, M. Schmittel, W. M. Heckl, *J. Phys. Chem. B* 2006, **110**, 10829.

36 L. Muller-Meskamp, S. Karthauser, R. Waser, M. Homberger, U. Simon, *Langmuir* 2008, **24**, 4577.

37 Y. L. Yang, C. Wang, *Curr. Opin. Colloid Interface Sci.*2009, *14*, 135.

38 P. Vanoppen, P. C. M. Grim, M. Rücker, S. De Feyter, G. Moessner, S. Valiyaveettil, K. Müllen, F. C. De Schryver, *J. Phys. Chem.* 1996, **100**, 19636.

39 C. Meier, M. Roos, D. Kunzel, A. Breitruck, H. E. Hoster, K. Landfester, A. Gross, R. J. Behm, U. Ziener, *J. Phys. Chem. C* 2010, **114,** 1268.

40 J. F. Dienstmaier, K. Mahata, H. Walch, W. M. Heckl, M. Schmittel, M. Lackinger, *Langmuir* 2010, **26**, 10708.